Stability of Ni Clusters and the Adsorption of CH4: First-Principles Calculations

2 AUTHORS:

Peter Ludwig Rodríguez-Kessler
Instituto Potosino de Investigación Científic…

5 PUBLICATIONS **2** CITATIONS

SEE PROFILE

Adán Rubén Rodríguez Domínguez
Universidad Autónoma de San Luis Potosí

**25** PUBLICATIONS **18** CITATIONS

SEE PROFILE

Stability of Ni Clusters and the Adsorption of CH$_4$: First-Principles Calculations

P. L. Rodríguez-Kessler[†] and A. R. Rodríguez-Domínguez*[,‡]

[†]Instituto Potosino de Investigación Científica y Tecnológica, San Luis Potosí 78216, México
[‡]Instituto de Física, Universidad Autónoma de San Luis Potosí, San Luis Potosí 78000, México

ABSTRACT: Structural, magnetic and adsorption properties of Ni$_n$ (n = 2−16, 21, 55) clusters have been investigated based on density funcional theory (DFT) with the spin polarized generalized gradient approximation, using the Perdew−Burke−Ernzerhof functional. The most stable isomers have been selected to study the adsorption of methane CH$_4$ and methyl CH$_3$. It is found that the CH$_4$ molecule adsorbs on the top site for all clusters considered. The most selective Ni$_n$ clusters are the tetrahedron (n = 4) and icosahedral clusters due to high-coordinated edge atoms (n = 13, 21, and 55). For CH$_3$, stronger adsorption tendencies were found with similar patterns. Our results show that clusters with n = 6, 10, and 13 with complete atomic shells are relatively more stable. Besides, they perform the lowest adsorption for CH$_3$, indicating that they possess such a desirable property of a higher carbon poisoning resistance, than for the rest of the clusters. This result can be understood in terms of the electronic stability and localization of the frontier molecular orbitals.
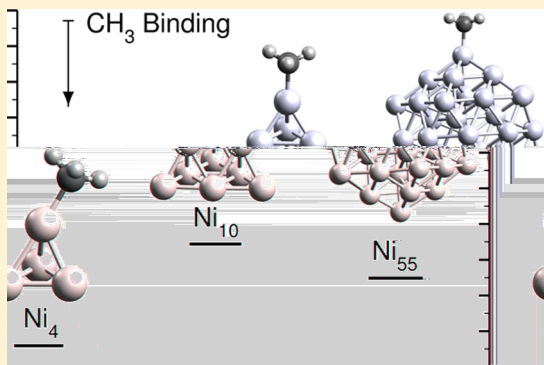
■ INTRODUCTION

Small clusters and nanoparticles have been widely studied in the past few years due to their high surface to volume ratio and enhanced reactivity properties compared with their bulk counterparts.[1] For example, gold nanoparticles are active catalyts although gold in the bulk is practically inert.[2,3] In catalytic reactions, they usually increase the selectivity and bond dissociation steps since they have more edge sites and low-coordinated atoms.[4] Although in some reactions the presence of edge sites on the surface of nanoparticles can reduce the specific catalytic activity,[5] they are useful for different reactions, such as decomposition of hydrocarbons and alcohols, which can serve as important hydrogen sources.[6,7]

Recently, much attention has been paid to the hydrogen production relating to the fuel cell technology.[8] In practice, hydrogen is produced from natural gas via steam reforming of methane, a process highly endothermic and very expensive, due to the high heat demand.[9] Among a wide range of heterogeneous catalyst, noble metal catalysts show higher activity and stability for this reaction, but the prohibitive cost and scarce resources makes their use very limited. On the other hand, Ni-based are promising catalysts in terms of cost and outstanding activity compared with noble-metals. However, the major problem of Ni-based systems is the strongly bonded carbon deposition on the catalyst surface which can deactivate the catalyst reducing its stability.[10]

In a previous work,[11] we have shown that small Rh clusters possess an excellent selectivity to catalytically adsorb and dissociate the acid rain precursor N$_2$O molecule. Furthermore, in the limit of going to arbit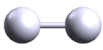rary large clusters, it was interesting to compare this effect with that of a flat (111) slab of same metal, which happened to be provided with a much more smaller selectivity as the corresponding to small clusters. The problem, however, appears when we begin to consider clusters of a bigger size, which could be more feasible from an experimental point of view. In another more recent work,[12] one of us could show, how FePt alloy clusters are able to catalytically and softly adsorb, and dissociate the O$_2$ molecule, and this effect could also be extended at the nanoparticle level. Since the properties of clusters depend on its size and structure, in this work, we explore the reactivity properties of pure Ni systems in order to identify the optimal structure to avoid carbon deposition on the catalyst surface.

Periodic DFT calculations have proven good agreement with the experimental data in the study of CH$_3$ and CH bonding fragments on Pt(111), which are known to be key intermediates in methane reactions.[13] Nave et al.[14] demonstrated that there is a strong preference on the Pt surfaces for CH$_3$ to bond on the top site, while on the Ni surfaces there is a preference for the hollow or bridge sites. In this context, top sites are more ideal to prevent the formation of strong carbon bindings. In the present paper, we performed DFT calculations for Ni clusters with n = 2−16, 21, and 55 atoms. Despite of a number of studies of 13-atom metallic clusters, the most stable structure of Ni$_{13}$ is kindly controversial. Density funcional theory studies indicated that a hcp structure is more stable than

Table 1. Lowest Energy Structures, Average Binding Energy ⟨E⟩, Bond Distances, Coordination Number ECN, and Magnetic Moment μ of Ni$_n$ Clusters with n = 2−7

Notation	Ni$_2$	Ni$_3$	Ni$_4$	Ni$_5$	Ni$_6$	Ni$_7$
Structure						
⟨E⟩ (eV/atom)	1.51	1.93	2.24	2.49	2.71	2.84
Bond length (Å)	2.08	2.20	2.20-2.32	2.25-2.33	2.28-2.35	2.31-2.34
ECN	1.0	2.0	2.93	3.57	3.97	4.28
d$_{av}$(Å)	2.08	2.20	2.27	2.31	2.31	2.32
μ (μ_B)	2.0	0.0	4.0	4.0	8.0	8.0

icosahedral structure.[15,16] We considered this an interesting finding, since Ni is located in the same column than Pd and Pt in the periodic table. Extensive studies of Pt clusters have been assigned by Kumar et al., suggesting planar, layered, pyramidal, cage, and cubic structures instead of icosahedral-like structures.[17] For Pd clusters, Khanna et al. showed that the icosahedral structure is around 0.14 eV above the ground state.[18] This could be one of the factors for the excellent catalytic properties exhibited by Pt, Pd, and Rh, among others. In the present work, we have undertaken a new search of the structures of Ni clusters to clarify if there are new structural conformations apart of Ni$_{13}$ and found new structural motifs from Ni$_{12}$ to Ni$_{14}$ clusters. We constructed the potential energy surface of Ni clusters, which is necessary to study their cluster adsorption properties and provides us the data that is necessary in our future studies of Ni systems. First, we discuss the stability of the bare Ni$_n$ clusters. Second, the adsorption energy and the geometry of the most favorable adsorption site on Ni$_n$ clusters. Finally, our main results and conclusions are given.

COMPUTATIONAL DETAILS

To determine the ground-state structures of Ni clusters, the configuration space was sampled by starting from several initial configuration and spin multiplicities. The initial structures were obtained starting from graph theory by the implementation of Wang[19] followed by a distance geometry optimization.[20] Since the number of spatial structures increases exponentially with size, for larger sizes, the consideration of all structures for calculation is very limited. For clusters with n = 8 up to 16, the initial geometries are generated by decoration of the $n − 1$ relaxed structures. The decoration consists of adding a single atom on all inequivalent sites on the cluster surface. This procedure, however, generates several structures from each size. In addition, to reduce the high computational cost, we only decorated the optimized structures which have $\Delta E < 1$ eV values of the relative energy difference from the global minina. Finally, the configuration with the lowest energy is taken as the ground state structure. For each size, the local minima of the potencial energy surface are proven by the harmonic vibrational frequencies. In order to study the adsorption properties of Ni$_n$ clusters, we considered various adsorption sites including top, hollow and bridge to approximate the CH$_4$ molecule to the clusters.

The calculations we reported herein are based on the Kohn−Sham (KS) density functional theory,[21,22] implemented through the code Vienna ab initio simulation package (VASP).[23,24] The exchange and correlation (XC) energy-functional is treated by using the Perdew−Burke−Ernzerhof (PBE) approximation.[25] The VASP code solves the spin-polarized KS equations by using the projector-augmented wave (PAW) method.[26] The wave functions are expanded in plane-wave basis sets with a cutoff energy of 450 eV. The atomic positions are relaxed self-consistently without restrictions in the symmetry by the conjugated gradient method algorithm, until the forces were practically smaller than 0.01 eV/Å for all atoms. We used a supercell with a distance of 10 Å of vacuum between periodic images, which is large enough to avoid their interaction. Due to the size of the supercell, only the Γ point is taken into account to represent the Brillouin zone.

In order to analyze the lowest-energy atomic structures and to describe how compact a cluster is, we use the effective coordination number (ECN) and averaged bond length[15,27] approach. The averaged bond length for the ith atom is defined as

$$d_{av}^i = \frac{\sum_{j=1}^n |R_i - R_j| \exp\left[1 - \left(\frac{|R_i - R_j|}{d_{av}^i}\right)\right]}{\sum_{j=1}^n \exp\left[1 - \left(\frac{|R_i - R_j|}{d_{av}^i}\right)\right]} \tag{1}$$

where R_i are the positions of the n atoms in the cluster. The initial value of d_{av}^i is taken as the shortest distance of the i atom at position R_i over all j atomic neighbors at positions R_j (with $j \neq i$). The final value is obtained self-consistently with a convergence criterion of 10^{-4} Å, that is, the obtained value of d_{av}^i is used as the initial value for the next iteration. The final value of d_{av} is obtained typically by using four iterations, and it is necessary to calculate ECN$_i$, defined as

$$ECN_i = \sum_{j=1}^n \exp\left[1 - \left(\frac{|R_i - R_j|}{d_{av}^i}\right)\right] \tag{2}$$

The average ECN and d_{av} for a particular configuration are obtained by

$$ECN = \frac{1}{n} \sum_{i=1}^n ECN_i \tag{3}$$

and

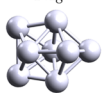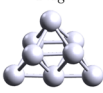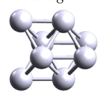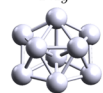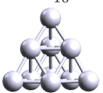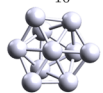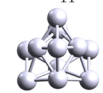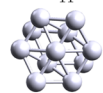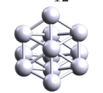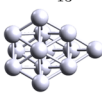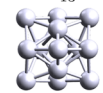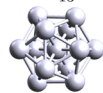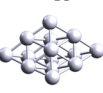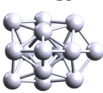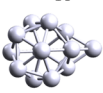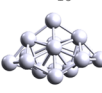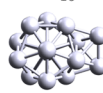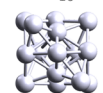$$d_{av} = \frac{1}{n} \sum_{i=1}^n d_{av}^i \tag{4}$$

The power of 6 and exponential form in d_{av} are used to obtain similar values for the standard coordination number CN for highly symmetric systems such as icosahedral clusters (CN = 6.46) and fcc crystalline solids (CN = 12).[28]

RESULTS AND DISCUSSION

For small Ni clusters, there are several theoretical studies that have documented the lowest-energy structures and their structural properties. For example, recent studies by Calaminici et al.[29,30] showed that the bond lengths of small nickel clusters

Table 2. Lowest Energy Structures, Relative Isomer Energy ΔE, Bond Distances, Coordination Number ECN, and Magnetic Moment μ of Ni_n Clusters That Have $n = 8-16$[a]

Notation	Ni_8^A	Ni_8^B	Ni_8^C	Ni_9^A	Ni_9^B	Ni_9^C
Structure						
ΔE(eV)	0.00 [2.93]	0.08	0.18	0.00 [3.03]	0.10	0.22
Bond length (Å)	2.28-2.67	2.26-2.43	2.29-2.36	2.21-2.38	2.27-2.41	2.31-2.56
ECN	4.55	4.46	4.49	4.60	4.61	5.00
d_{av}(Å)	2.34	2.33	2.34	2.34	2.33	2.35
μ (μ_B)	8.0	8.0	8.0	8.0	8.0	8.0

Notation	Ni_{10}^A	Ni_{10}^B	Ni_{10}^C	Ni_{11}^A	Ni_{11}^B	Ni_{11}^C
Structure						
ΔE(eV)	0.00 [3.11]	0.25	0.29	0.00 [3.16]	0.07	0.22
Bond length (Å)	2.27-2.41	2.28-2.57	2.30-2.60	2.28-2.59	2.30-2.52	2.31-2.44
ECN	4.71	5.06	5.23	5.28	5.33	5.25
d_{av}(Å)	2.32	2.35	2.36	2.35	2.35	2.35
μ (μ_B)	8.0	8.0	8.0	8.0	8.0	8.0

Notation	Ni_{12}^A	Ni_{12}^B	Ni_{12}^C	Ni_{13}^A	Ni_{13}^B	Ni_{13}^C
Structure						
ΔE(eV)	0.00 [3.20]	0.10	0.37	0.00 [3.25]	0.13	0.22
Bond length (Å)	2.32-2.47	2.30-2.55	2.28-2.51	2.30-2.43	2.29-2.55	2.29-2.47
ECN	5.47	5.53	5.89	5.48	5.69	6.38
d_{av}(Å)	2.36	2.36	2.39	2.36	2.37	2.41
μ (μ_B)	8.0	8.0	8.0	10.0	10.0	8.0

Notation	Ni_{14}^A	Ni_{14}^B	Ni_{14}^C	Ni_{15}^A	Ni_{15}^B	Ni_{15}^C
Structure						
ΔE(eV)	0.00 [3.28]	0.01	0.18	0.00 [3.32]	0.19	0.23
Bond length (Å)	2.30-2.46	2.28-2.60	2.28-2.50	2.29-2.57	2.30-2.58	2.29-2.64
ECN	5.53	5.81	6.32	5.95	6.42	5.92
d_{av}(Å)	2.36	2.38	2.40	2.38	2.41	2.38
μ (μ_B)	10.00	12.00	10.00	12.00	12.00	12.00

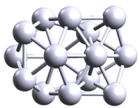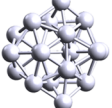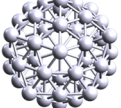[a]$\langle E \rangle$ of the ground state structures is given in square brackets.

with $n = 2-5$ can be correctly predicted using a GGA XC functional in fair good agreement with the experimental data. Xie et al.[31] have studied the structural and magnetic properties of the Ni_n ($n = 2-13$) clusters using the BLYP XC functional and found that the Jahn−Teller effect plays an important role in determining the ground state of certain geometric structures. Wen-Cai Lu et al.[32] calculated the structures of the Ni_n ($n = 2-30$) clusters using the PBE XC energy functional and found that the structures of the Ni_n clusters exhibit a double-icosahedron-based motif. In Table 1 we present the lowest-energy structures of Ni clusters with $n = 2-7$ along with the bond lengths and magnetic moments. For the Ni_2 dimer, our calculated bond distance is 2.08 Å, in close agreement with the experimental bond length of 2.15 Å.[33] From different DFT computational methods, the reported bond lengths are 2.148 Å using the TZVP-GGA/PW86 method,[29] 2.11 Å from GGA/BLYP approximations,[31] and 2.09 Å from GGA/PW-91 plane-wave method,[34] among others.

The stable structures of Ni_{3-6} are triangle, tetrahedron, tetrahedral bipyramid, and octahedron, respectively. From early DFT calculations, a square pyramid was identified as the ground state structure for Ni_5.[32,35] Nevertheless, it was predicted by the experiment[36] and theoretical studies,[29,30] a trigonal bipyramid to represent the ground state. We found that the trigonal bipyramid (with 4 μ_B) is 0.02 eV more stable than the square pyramid (with 6 μ_B). In accordance with the results of Parks et al., the ground state structure of Ni_6 is an octahedron with O_h symmetry, while the structures of Ni_7 and Ni_8 can be formed by capping one or two atoms to the Ni_6 octahedron.[36] Ni_9 is a tricapped trigonal prism.[37] Ni_{10} is a tetrahedron with a T_d symmetry. The structure of Ni_{11} has a C_{2v} symmetry in accordance with Posada-Amarillas and Garzón.[38] In contrast, Lu et al. found a trilayered structure with a 3−5−3 stacking for Ni_{11}, but our results showed that it is 0.22 eV less stable than the C_{2v} structure (see Table 2) . From Ni_{11} to Ni_{14}, we found that the icosahedral motif is not energetically preferable, although in most of the previous studies, the icosahedral structures were assigned as the ground state.[31,32,34,39,40] For example, Ni_{12} has a three layered 3−6−3 stacking structure that is 0.37 eV more stable than the icosahedral one. Despite many studies of Ni clusters, for Ni_{13}, extensive studies of 13-atom metallic clusters reported the hcp structure as more stable than the icosahedral one.[15,16] In accordance with Chou et al., the ground state structure of Ni_{13}

C

has a C_{3v} symmetry and 10 μ_B of magnetic moment. The values of ECN = 5.48 and d_{av} = 2.36 are also found in close agreement for this structure.[15] For Ni_{13}, we found that the icosahedron is 0.22 eV over the global minimun, while for Ni_{14}, the icosahedral structure is more stable (ΔE = 0.18 eV). It is important to note that the Ni_{13} (1–3–6–3) and Ni_{14} (1–3–6–3–1) layered clusters can be formed by capping the Ni_{12} cluster with one or two atoms. The structure of Ni_{15} is not longer connected to Ni_{14}. Rather, it can be formed by adding one atom on the second isomer of Ni_{14}. Additionally and for comparison, we also included larger Ni clusters with n = 16, 21, and 55, as shown in Table 3, which have icosahedral structures, in accordance with theoretical and experimental findings.[41−43]

Table 3. Lowest Energy Structures, Average Binding Energy ⟨E⟩, Bond Distances, Coordination Number N, and Magnetic Moment μ of Ni_n Clusters with n = 16, 21, and 55[a]

Notation	Ni_{16}	Ni_{21}	Ni_{55}
Structure			
⟨E⟩ (eV/atom)	3.35	3.50	3.93
Bond length (Å)	2.31-2.65	2.25-2.73	2.28-2.54
ECN	6.47	6.99	8.39
d_{av}(Å)	2.40	2.42	2.44
μ (μ_B)	12.0	18.0	40.0

[a]Distances are given in Å.

The calculated average binding energy ⟨E⟩ of Ni_n clusters is defined as

$$\langle E \rangle = (E_T[Ni_n] - nE_T[Ni])/n \qquad (5)$$

Our results show that ⟨E⟩ increases a bit rapidly with the cluster size n up to $n \leq 6$ then continues increasing with $n > 6$ but rather gradually, as shown in Figure 1. In order to describe
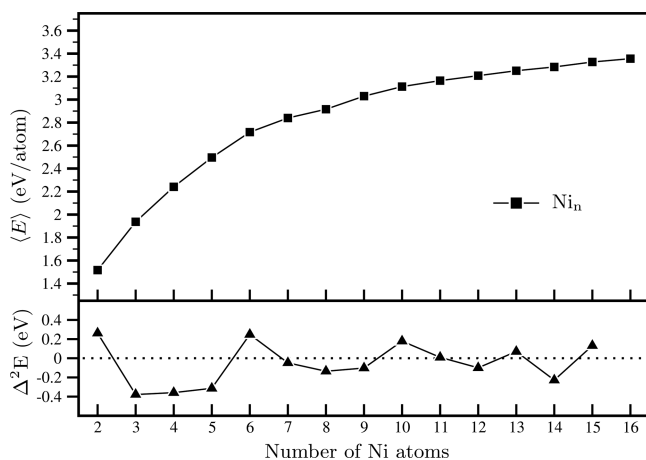

Figure 1. Average binding energy ⟨E⟩ (top) and second energy difference $\Delta_2 E$ (bottom) of the most stable structures of Ni_n clusters.

the stability of Ni_n clusters, we have defined two different energies. These energies are the binding energy

$$E_{bind} = E_T[Ni_n] - E_T[Ni_{n-1}] - E_T[Ni] \qquad (6)$$

and the second-order in energy difference

$$\Delta_2 E = E_T[Ni_{n+1}] + E_T[Ni_{n-1}] - 2E_T[Ni_n] \qquad (7)$$

To characterize the molecular adsorptions, the adsorption energy is defined as

$$E_{ads} = E_T[CH_4 - Ni_n] - E_T[Ni_n] - E_T[CH_4] \qquad (8)$$

where $E_T[CH_4]$, $E_T[Ni_n]$, and $E_T[CH_4-Ni_n]$ are the total energies of the bare CH_4 molecule, the relaxed free Ni_n cluster in the gas phase, and the CH_4-Ni_n complex, respectively. From the curve of $\Delta_2 E$ in Figure 1, the local peaks are localized at n = 6, 10, 13, and possibly 15, indicating that these clusters are relatively more stable. Another useful physical quantity that can reflect the relative stability is the energy gain E_{bind} upon addition of an extra Ni atom to the clusters, as shown in Figure 2. Since the total energies are negative, a local minimum in the
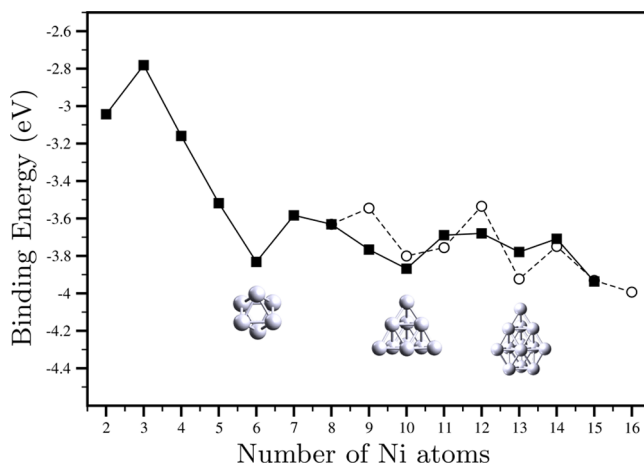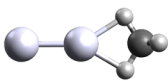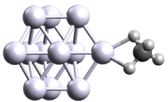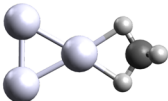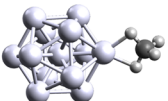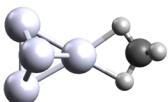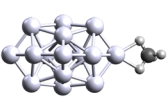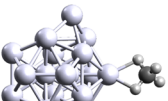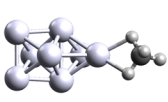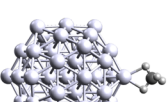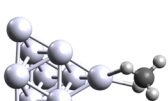

Figure 2. Binding energy E_{bind} of the most stable structures of Ni_n clusters (squares). E_{bind} of icosahedral structures (circles).

E_{bind} curve can be seen for n = 6, 10, and 13; these are the magic clusters with atomically closed shells and symmetric structures, such as an octahedron, layered triangular prism, and hcp structure, respectively, suggesting that these clusters are more stable compared to their neighbors. For comparison, we plotted the icosahedron growth (on circles) and found a remarkable stability for the Ni_{13} cluster. In ref 32, based on a second difference cluster energy plot, the Ni_{10} and Ni_{11} clusters have been also considered as magic, since they are close in stability. We found the same trend considering the icosahedral growth. In the next section, the results of the adsorption properties of Ni_n clusters and the effect of the cluster stability are discussed.

Adsorption of a CH_4 on Ni Clusters. In Table 4, we present the calculations of CH_4 adsorption on the most stable isomers of the selected Ni_n sizes that have n = 2, 3, 4, 6, 10, 12, 13, 15, 21, and 55. The adsorption of CH_4 is investigated at different high symmetry sites, including top, bridge, and hollow. The top site is found to be more stable than the bridge site in all cases considered (see Table 4). We found the same structural conformations for CH_4-Ni_n complexes than that of the isolated clusters. Low adsorption energy values are found, ranging from −0.17 to −0.47 eV and small changes in the cluster bond lengths are also observed. For example, for CH_4–Ni_2 (2a complex), the Ni−Ni bond length is 2.12 Å, which is slightly larger than the bare Ni_2 dimer (2.08 Å). The Ni−C bond length is 2.17 Å and the C−H bond length is 1.12 Å, which is larger than that of free CH_4 molecule (1.09 Å), which is consistent with the high C−H bond stability. The total magnetic moment is unchanged for all clusters considered. We

Table 4. Structures of CH_4–Ni_N Complexes, the Total Magnetic Moment μ, Adsorption Energy E_{ads}, and the Coordination of the Adsorption Site $N_s^{\ a}$

Structure	Label	μ (μ_B)	E_{ads} (eV)	N_s	Structure	Label	μ (μ_B)	E_{ads} (eV)	N_s
	2a	2.00	-0.35	1		12a	8.00	-0.26	4
	3a	0.00	-0.30	2		13a	8.00	-0.30	6
	4a	4.00	-0.47	3		15a	12.00	-0.21	4
	6a	6.00	-0.18	4		21a	18.00	-0.27	6
	8a	8.00	-0.26	4		55a	40.00	-0.17	6
	10a	8.00	-0.21	3					

^{a}Lower case letters are used to label the adsorbed complexes.

found that the deepest adsorption is performed by Ni_4 on the top site, with an adsorption energy of -0.47 eV/CH_4. Due to high-coordinated sites, N_s, Ni_{13}, Ni_{21}, and Ni_{55} were also found to be selective for CH_4, since the adsorption energy of CH_4 has small changes with cluster size. We investigated the adsorption of the CH_3 subproduct and found a stronger size-dependent adsorption, as shown in Figure 3. From this curve, the deepest adsorptions of CH_4 occur for some even-sized clusters (those with n = 4, 8, and 12). On the other hand, weak CH_3 adsorptions occur for n = 6, 10, 13, and 55, with E_{ads} ranging from -1.81 (Ni_{10}) to -1.99 eV/CH_3 (Ni_{55}). Those sizes correspond to magic clusters. Interestingly, by removing a single hydrogen atom from the adsorbed complex CH_4–Ni_n, they perform a top site CH_3 binding.

In accordance with the high electronic stability, we expect that they possess more carbon poisoning resistance. For Ni_{12} and Ni_{15}, CH_3 preferentially binds on the bridge site performing a deeper adsorption as shown in the adsorption plot. In order to illustrate our findings, CH_3 adsorptions on Ni_4, Ni_{10}, Ni_{12} and Ni_{15} are illustrated in Figure 4, in spite of the deeper adsorptions, we included some bond distances in the Figure.

In order to determine if the reactivity of clusters are related to their electronic properties, in Figure 5 we illustrate the highest occupied molecular orbitals of Ni_{10} and Ni_{12}. One can observe, that the tetrahedral structure of Ni_{10} performs less
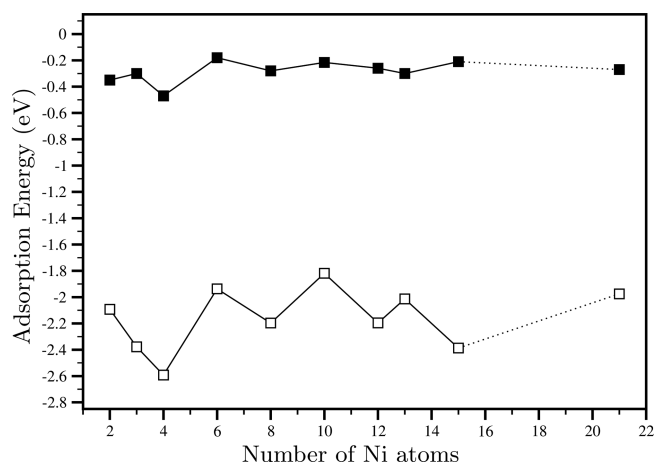
Figure 3. Adsorption energy E_{ads} for CH_4 (closed squares) and CH_3 (open squares) on Ni_n clusters.

localization on the edge atom sites. From this observation, we expect smaller electrostatic interactions of the HOMO orbitals, degrading the adsorption of CH_3.[44] On the other hand Ni_{12} possesses more localization on the cluster surface. We also attribute this property to the low coordination of Ni_{10} (ECN = 4.71) in comparison to Ni_{12} (ECN = 5.47). These results suggest a strong structural dependence on the electronic
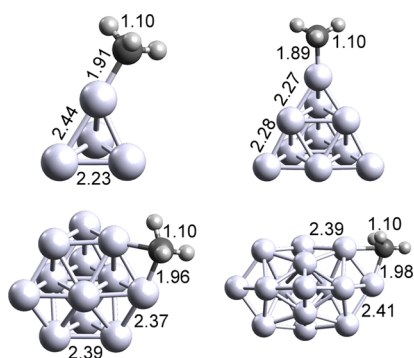
Figure 4. CH_3 adsorption on Ni_4, Ni_{10}, Ni_{12}, and Ni_{15} clusters. Distances are given in Å.
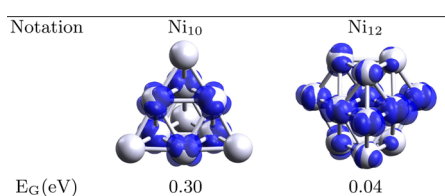
Figure 5. Frontier molecular orbitals of Ni_{10} and Ni_{12} clusters (0.02 $eV/Å^{3/2}$ of isosurface value). E_G denotes the energy between the highest occupied and the lowest unoccupied molecular orbitals.

properties of Ni_n clusters and support that magic clusters are less reactive, increasing their carbon poisoning resistance. Furthermore, the band gap E_G of Ni_{10} is larger than that of Ni_{12}, suggesting a higher electronic stability. These findings motivate us going into further works and studying atom impurities inside magic-number clusters. In this context, Skomski and Sellmyer[45] found that magnetic impurities in magic-cluster hosts lead to a reduction of the band gap splitting, which affects the optical properties. Those effects are still not revealed from a catalytic point of view and further investigations of the catalytic properties of clusters with closed-electronic shells might be considered for future works.

◼ CONCLUSIONS

The goal of this work has been to study CH_4 adsorption on Ni_n clusters consisting of $n = 2-16$, 21, and 55 atoms in the framework of the spin-polarized density functional theory. The calculated binding energies of Ni_n clusters revealed the most stable cluster sizes. We found that there are other more stable structural conformations than the icosahedral ones, to represent the ground state structures for Ni_n clusters with $n \leq 15$. Based on the most stable structures of Ni_n clusters we calculated the active sites and adsorption energies of an interacting CH_4 molecule. The preferential adsorption corresponds to the top site. We found adsorption energies ranging from -0.17 to -0.47 eV in all clusters considered; nevertheless, the binding of the CH_3 subproduct has a strong size-dependent effect. We found that the magic-clusters are more suitable to adsorb CH_4 since they possess low adsorption to CH_3 and therefore more carbon poisoning resistance in real reaction conditions. These results prompt us to consider and explore before long the effect of atomic impurities on magic Ni_n clusters in order to improve their catalytic properties.

◼ AUTHOR INFORMATION

Corresponding Author
*E-mail: adnrdz@ifisica.uaslp.mx.

Notes
The authors declare no competing financial interest.

◼ REFERENCES

(1) Xiao, L.; Wang, L. Structures of Platinum Clusters: Planar or Spherical? *J. Phys. Chem. A* **2004**, *108*, 8605−8614.

(2) Hayashi, T.; Tanaka, K.; Haruta, M. Selective Vapor-Phase Epoxidation of Propylene over Au/TiO₂ Catalysts in the Presence of Oxygen and Hydrogen. *J. Catal.* **1998**, *178*, 566−575.

(3) Chen, Y.; Crawford, P.; Hu, P. Recent Advances in Understanding CO Oxidation on Gold Nanoparticles Using Density Functional Theory. *Catal. Lett.* **2007**, *119*, 21−28.

(4) Oemry, F.; Padama, A. A. B.; Kishi, H.; Kunikata, S.; Nakanishi, H.; Kasai, H.; Maekawa, H.; Osumi, K.; Sato, K. Effects of Cluster Size on Platinum-Oxygen Bonds Formation in Small Platinum Clusters. *Jpn. J. Appl. Phys.* **2012**, *51*, 035002.

(5) Shao, M.; Peles, A.; Shoemaker, K. Electrocatalysis on Platinum Nanoparticles: Particle Size Effect on Oxygen Reduction Reaction Activity. *Nano Lett.* **2011**, *11*, 3714−3719.

(6) Rostrup-Nielsen, J. R. Conversion of Hydrocarbons and Alcohols for Fuel Cells. *Phys. Chem. Chem. Phys.* **2001**, *3*, 283−288.

(7) Mehmood, F.; Greeley, J.; Curtiss, L. A. Density Functional Studies of Methanol Decomposition on Subnanometer Pd Clusters. *J. Phys. Chem. C* **2009**, *113*, 21789−21796.

(8) Wu, H.; La Parola, V.; Pantaleo, G.; Puleo, F.; Venezia, A. M.; Liotta, L. F. Ni-Based Catalysts for Low Temperature Methane Steam Reforming: Recent Results on Ni-Au and Comparison with Other Bi-Metallic Systems. *Catalysts* **2013**, *3*, 563−583.

(9) Rogatis, L. D.; Montini, T.; Cognigni, A.; Olivi, L.; Fornasiero, P. Methane Partial Oxidation on NiCu-Based Catalysts. *Catal. Today* **2009**, *145*, 176−185.

(10) Tomishige, K. Oxidative Steam Reforming of Methane over Ni Catalysts Modified with Noble Metals. *J. Jpn. Pet. Inst.* **2007**, *50*, 287−298.

(11) Rodríguez-Kessler, P.; Rodríguez-Domínguez, A. N₂O Dissociation on Small Rh Clusters: A Density Functional Study. *Comput. Mater. Sci.* **2015**, *97*, 32−35.

(12) Rodríguez-Kessler, P.; Ricardo-Chávez, J. Structures of FePt Clusters and their Interactions with the O₂ Molecule. *Chem. Phys. Lett.* **2015**, *622*, 34−41.

(13) Karp, E. M.; Silbaugh, T. L.; Campbell, C. T. Energetics of Adsorbed CH_3 and CH on Pt(111) by Calorimetry: Dissociative Adsorption of CH₃I. *J. Phys. Chem. C* **2013**, *117*, 6325−6336.

(14) Nave, S.; Tiwari, A. K.; Jackson, B. Methane Dissociation and Adsorption on Ni(111), Pt(111), Ni(100), Pt(100), and Pt(110)-(1 × 2): Energetic Study. *J. Chem. Phys.* **2010**, *132*, 054705.

(15) Chou, J. P.; Hsing, C. R.; Wei, C. M.; Cheng, C.; Chang, C. M. Ab Initio Random Structure Search for 13-Atom Clusters of FCC Elements. *J. Phys.: Condens. Matter* **2013**, *25*, 125305.

(16) Aguilera-Granja, F.; Longo, R. C.; Gallego, L. J.; Vega, A. Structural and Magnetic Properties of X12Y (X, Y = Fe, Co, Ni, Ru, Rh, Pd, and Pt) Nanoalloys. *J. Chem. Phys.* **2010**, *132*, 184507.

(17) Kumar, V.; Kawazoe, Y. Evolution of Atomic and Electronic Structure of Pt Clusters: Planar, Layered, Pyramidal, Cage, Cubic, and Octahedral Growth. *Phys. Rev. B* **2008**, *77*, 205418.

(18) Köster, A. M.; Calaminici, P.; Orgaz, E.; Roy, D. R.; Reveles, J. U.; Khanna, S. N. On the Ground State of Pd13. *J. Am. Chem. Soc.* **2011**, *133*, 12192−12196.

(19) Wang, Y.; George, T. F.; Lindsay, D. M.; Beri, A. C. The Hückel Model for Small Metal Clusters. I. Geometry, Stability, and Relationship to Graph Theory. *J. Chem. Phys.* **1987**, *86*, 3493−3499.

(20) Moré, J.; Wu, Z. Global Continuation for Distance Geometry Problems. *SIAM J. Control* **1997**, *7*, 814−836.

(21) Hohenberg, P.; Kohn, W. Inhomogeneous Electron Gas. *Phys. Rev.* **1964**, *136*, B864−B871.

(22) Kohn, W.; Sham, L. J. Self-Consistent Equations Including Exchange and Correlation Effects. *Phys. Rev.* **1965**, *140*, A1133−A1138.

(23) Kresse, G.; Hafner, J. Ab Initio Molecular Dynamics for Liquid Metals. *Phys. Rev. B* **1993**, *47*, 558−561.

(24) Kresse, G.; Furthmüller, J. Efficient Iterative Schemes for Ab Initio Total-Energy Calculations Using a Plane-Wave Basis Set. *Phys. Rev. B* **1996**, *54*, 11169−11186.

(25) Perdew, J. P.; Burke, K.; Ernzerhof, M. Generalized Gradient Approximation Made Simple. *Phys. Rev. Lett.* **1997**, *78*, 1396−1396.

(26) Blöchl, P. E. Projector Augmented-Wave Method. *Phys. Rev. B* **1994**, *50*, 17953−17979.

(27) Hoppe, R. The Coordination Number - an "Inorganic Chameleon. *Angew. Chem.* **1970**, *9*, 25−34.

(28) Piotrowski, M. J.; Piquini, P.; Da Silva, J. L. F. Density Functional Theory Investigation of 3*d*, 4*d*, and 5*d* 13-Atom Metal Clusters. *Phys. Rev. B* **2010**, *81*, 155446.

(29) López Arvizu, G.; Calaminici, P. Assessment of Density Functional Theory Optimized Basis Sets for Gradient Corrected Functionals to Transition Metal Systems: The Case of Small Ni_n ($n \le$ 5) Clusters. *J. Chem. Phys.* **2007**, *126*, 194102.

(30) Calaminici, P. Is the Trend of the Polarizability per Atom for all Small 3*d* Transition Metal Clusters the Same? The case of Ni_n ($n \le$ 5) clusters. *J. Chem. Phys.* **2008**, *128*, 164317.

(31) Xie, Z.; Ma, Q.-M.; Liu, Y.; Li, Y.-C. First-Principles Study of the Stability and Jahn-Teller Distortion of Nickel Clusters. *Phys. Lett. A* **2005**, *342*, 459−467.

(32) Song, W.; Lu, W.-C.; Wang, C.; Ho, K. Magnetic and Electronic Properties of the Nickel Clusters Ni_n (n = 2−30). *Comput. Theor. Chem.* **2011**, *978*, 41−46.

(33) Pinegar, J. C.; Langenberg, J. D.; Arrington, C. A.; Spain, E. M.; Morse, M. D. Ni_2 Revisited: Reassignment of the Ground Electronic State. *J. Chem. Phys.* **1995**, *102*, 666−674.

(34) Deshpande, M. D.; Roy, S.; Kanhere, D. G. Equilibrium Geometries, Electronic Structure, and Magnetic Properties of Ni_nSn Clusters (n = 1−12). *Phys. Rev. B* **2007**, *76*, 195423.

(35) Lu, Q. L.; Luo, Q. Q.; Chen, L. L.; Wan, J. G. Structural and Magnetic Properties of Ni_n (n = 2−21) Clusters. *Eur. Phys. J. D* **2011**, *61*, 389−396.

(36) Parks, E. K.; Zhu, L.; Ho, J.; Riley, S. J. The Structure of Small Nickel Clusters. I. Ni_3-Ni_{15}. *J. Chem. Phys.* **1994**, *100*, 7206−7222.

(37) Luo, C. A. Possible Packing Sequence of Nickel Clusters: Ni_{13}-Ni_{32}. *New J. Phys.* **2002**, *4*, 10.1−10.8.

(38) Posada-Amarillas, A.; Garzón, I. L. Vibrational Analysis of Ni_n Clusters. *Phys. Rev. B* **1996**, *54*, 10362−10365.

(39) Grigoryan, V. G.; Springborg, M. Structural and Energetic Properties of Nickel Clusters: $2 \le N \le 150$. *Phys. Rev. B* **2004**, *70*, 205415.

(40) Reddy, B. V.; Nayak, S. K.; Khanna, S. N.; Rao, B. K.; Jena, P. Physics of Nickel Clusters. 2. Electronic Structure and Magnetic Properties. *J. Phys. Chem. A* **1998**, *102*, 1748−1759.

(41) Wang, Q.; Lim, K.; Yang, S.-W.; Yang, Y.; Chen, Y. Atomic Carbon Adsorption on Ni Nanoclusters: a DFT Study. *Theor. Chem. Acc.* **2011**, *128*, 17−24.

(42) Klots, T. D.; Winter, B. J.; Parks, E. K.; Riley, S. J. Icosahedral Structure in Hydrogenated Cobalt and Nickel Clusters. *J. Chem. Phys.* **1991**, *95*, 8919−8930.

(43) Pellarin, M.; Baguenard, B.; Vialle, J.; Lermé, J.; Broyer, M.; Miller, J.; Perez, A. Evidence for Icosahedral Atomic Shell Structure in Nickel and Cobalt Clusters. Comparison with Iron Clusters. *Chem. Phys. Lett.* **1994**, *217*, 349−356.

(44) Lei, X. L.; Wu, M. S.; Liu, G.; Xu, B.; Ouyang, C. Y. The Role of Cu in Degrading Adsorption of CO on the Pt_nCu Clusters. *J. Phys. Chem. A* **2013**, *117*, 8293−8297.

(45) Skomski, R.; Sellmyer, D. J. Magnetic Impurities in Magic-Number Clusters. *J. Appl. Phys.* **2007**, *101*, 09G524.